

Ultrastability and Enhanced Stiffness of ~ 6 nm TiO_2 Nanoanatase and Eventual Pressure-Induced Disorder on the Nanometer Scale

V. Pischedda, G. R. Hearne, A. M. Dawe, and J. E. Lowther

*DST-NRF Center of Excellence in Strong Materials and School of Physics, University of the Witwatersrand,
P.O. Wits, 2050, Johannesburg, South Africa*

(Received 9 August 2005; published 27 January 2006)

At 300 K ultrafine ~ 6 nm grain-size nanoanatase retains its structural integrity up to 18 GPa. There is progressive pressure-induced structural disorder to a highly disordered state at $P > 18$ GPa. Signatures of short-range order persist to well beyond 18 GPa in both the synchrotron-x-ray diffraction and Raman data. Molecular dynamics simulations suggest disorder initiated in the surface shell of a nanograin with crystallinity being retained in the core. A bulk modulus $B_0 = 237 \pm 3$ GPa for the nanoanatase ($\sim 30\%$ higher than the bulk value) is derived from the P - V data, concordant with the MD calculations.

DOI: [10.1103/PhysRevLett.96.035509](https://doi.org/10.1103/PhysRevLett.96.035509)

PACS numbers: 61.46.-w, 61.50.Ks, 63.22.+m, 64.70.Nd

Polymorphs of TiO_2 have had considerable impact over a broad range of scientific inquiry. Typical examples are the following: (i) Anatase TiO_2 is a wide band-gap material of indispensable importance in advanced electrochemical dye solar cells [1]. (ii) It has proven to be an effective support as a source of oxygen for nanogold catalysts used for noxious CO oxidation to innocuous CO_2 at low (room) temperatures [2]. (iii) There are very recent reports of intrinsic room-temperature ferromagnetism in insulating cobalt doped anatase- TiO_2 thin films, and this is expected to have exciting implications for new-generation semiconductor spin-electronic (spintronic) devices [3]. (iv) Last, and perhaps more pertinent to this presentation, is the fairly recent discovery that one of the high pressure-temperature structural phases of TiO_2 is the least compressible (hardest) known metal-oxide phase measured to date [4].

There is now an intense interest in ultrafine nanometer-sized materials since they exhibit chemical, physical, and mechanical properties significantly different (and often considerably improved) compared to that of the coarser-grained counterparts [5]. The focus of this work is on the stability and mechanical properties of ultrafine nanoanatase TiO_2 . Nanophase starting materials are considered important in the high P - T processing of advanced engineering materials. The high surface-to-volume ratio leads to enhanced processing and mechanical properties compared to the bulk. For example, there is improved reactivity, low P - T sinterability, and stability (superplasticity and fracture toughness) [6]. Consequently, fully densified compacts may be developed for relatively cheap long-lifetime cutting-grinding tools.

We consider the structural integrity of ultrafine 6 nm grain-size anatase TiO_2 under extreme conditions. This is partly to ascertain the thermodynamic conditions under which the nanostructured starting material (nanoanatase) may convert to an ultrahard oxide (e.g., cotunnite phase) as in the case of the macrocrystalline analog [4]. The large surface-to-volume ratio in the nanomaterial has implica-

tions for the onset P - T conditions to new crystalline phases. It is of interest to have such crystalline-to-crystalline transitions occur at industrially accessible P - T conditions. To this end, ultrafine nanoanatase has been investigated by synchrotron x-ray diffraction along the room-temperature isotherm up to 30 GPa. The structural stability has been monitored and bulk modulus (compressibility) extracted for comparison with that of the macrocrystalline analog.

The structural stability of bulk anatase at 300 K is well known. It undergoes a crystallographic transition from the tetragonal structure to the orthorhombic α - PbO_2 -type structure at $P = 2$ –5 GPa, and then to the monoclinic baddeleyite structure at 12–15 GPa [7]. However, in the nanophase material there have already been indications of radically different behavior [8–11]. Previous Raman studies have hinted that nanophase TiO_2 anatase (~ 6 and 12 nm grain sizes) remains stable to much higher pressures than the bulk, before either transforming directly to the baddeleyite structure or amorphizing, depending on the starting grain size [8–11]. The analyses of these high pressure Raman data have led to suggestions that, compared with bulk anatase, there is a decrease or similar compressibility for the 6, 7–11, and 12 nm nanophase material. However, Raman mode shifts are not a direct and unambiguous way of determining compressibility [9].

The elastic stiffness, and therefore the bulk modulus, is best obtained from isothermal x-ray diffraction studies over a range of pressures. A previous x-ray powder diffraction study of nanocrystalline anatase of 30–40 nm average grain size has shown that the bulk modulus is about 35% larger than that of the macrocrystalline counterpart [10]. The nanoanatase of these dimensions remains stable to ~ 18 GPa before a crystalline-to-crystalline transition ensues from anatase to the baddeleyite structure. To date, though, there has been no x-ray diffraction characterization of the nanoanatase structure at high pressures for grain sizes less than 30 nm. This is accomplished in this

work on the ultrafine version of this material, namely, ~ 6 nm diameter nanograins. Synchrotron x-ray data in conjunction with results of a Raman investigation have been obtained for this material pressurized in a Merrill-Bassett-type diamond-anvil cell. We have deliberately steered away from *in situ* heating of the sample at high pressure to avoid any grain coarsening likely to occur under high P - T conditions. The experimental investigation has been complemented by molecular dynamics (MD) simulations of the pressure response of nanoparticles having comparable minute grain sizes $d = 4$ nm.

TiO₂ nanoparticles were synthesized from TiCl₄ by the hydrothermal method [12], and characterization of the nanoanatase starting material was made by using both TEM and x-ray diffraction. The Scherrer formula has been used to estimate an average particle size of diameter $d = 6 \pm 1$ nm from the (101) and (200) diffraction line-widths. Synchrotron x-ray diffraction patterns have been collected in the pressure range 1 to 30 GPa at intervals of about 2 GPa ($\lambda = 0.4167$ Å, ID-9 beam line at ESRF Grenoble, France). A Fluorinert FC70—FC77 (1:1) mixture has been used as a pressure-transmitting medium and pressure determined from the ruby R1-luminescence line shift. The FIT2D software package [13] was then used to integrate the diffraction rings into one-dimensional patterns. These were subsequently analyzed by the GSAS code [14] to extract the cell parameters from a full-profile fitting analysis. Details of the Raman experiments are similar to those presented by Hearne *et al.* [9] on larger grains ($d \sim 12$ nm) of nanoanatase.

Figure 1 displays angle dispersive x-ray diffraction spectra taken at pressure for the 6 nm nano-TiO₂ sample. The nanoanatase phase is stable to 18 GPa, after which evidence of structural disorder begins to set in as suggested by

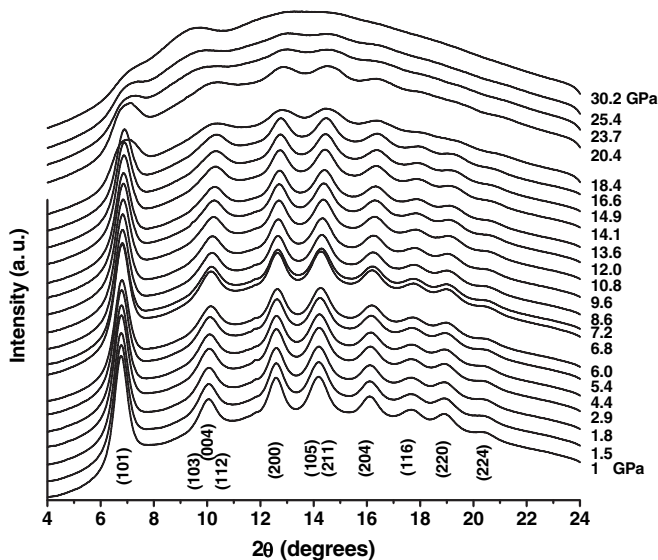


FIG. 1. High pressure powder x-ray diffraction spectra of nanoanatase up to 30 GPa at room temperature.

excessive peak broadening and a diffuse halo emerging. The latter, manifested as an increase in background intensity, is supposed to signal the onset of disorder on a large length scale comparable to grain-size dimensions. The degree of disorder increases progressively at pressures beyond 18 GPa. Anatase reflections at low angles are excessively broadened while those at high angles are barely discerned. At $P \sim 30$ GPa most of the diffraction lines disappear, and a hump supposed to be characteristic of the highly disordered phase appears between 8° and 12° of 2θ . The material can be considered progressively more disordered and eventually near-amorphous at pressures beyond ~ 21 GPa, as corroborated by the Raman spectroscopy data shown in Fig. 2. The weak and broad Bragg reflections and Raman band signatures of the anatase structure remain present in the spectra to well beyond $P = 18$ GPa where the onset of disorder is supposed to occur (see Figs. 1 and 2). The highly disordered or amorphous phase is quenchable after release of pressure.

MD simulations have been performed on a 4 nm TiO₂ anatase particle consisting of 2945 atoms. A simple Buckingham potential [15] was employed to model the interatomic potentials within a constant pressure simulation chosen to represent the pressure on a single nanoparticle with no direct interaction between the particles. Such a simple potential is expected to perform quite reasonably for the lower density structures such as TiO₂ anatase although it is not applicable to the study of the high pressure (e.g., cotunnite) phases [16]. For all simulations a starting box of 10 nm dimension, well in excess of the nanoparticle volume, was initially chosen. Even for higher pressures in excess of 30 GPa the reduced size of the MD box always remained well in excess of the nanoparticle volume. All simulations were performed at 0 K with all atoms relaxed, convergence criteria being both near-zero velocity for all atoms and a stable total energy.

In Fig. 3 we show the calculated radial distribution function (RDF) of the nanoparticle for various pressures.

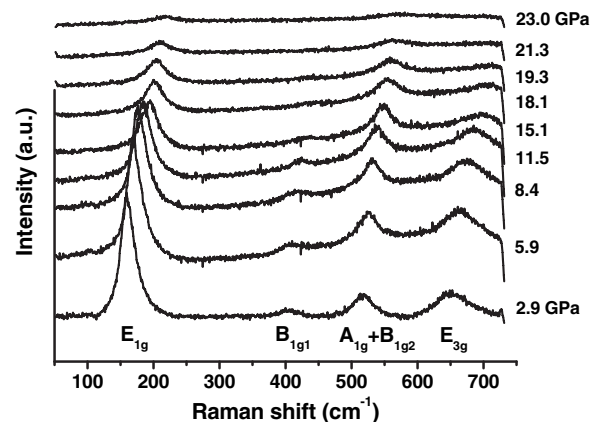


FIG. 2. Raman spectra at room temperature of nanoanatase up to high pressures of 23 GPa.

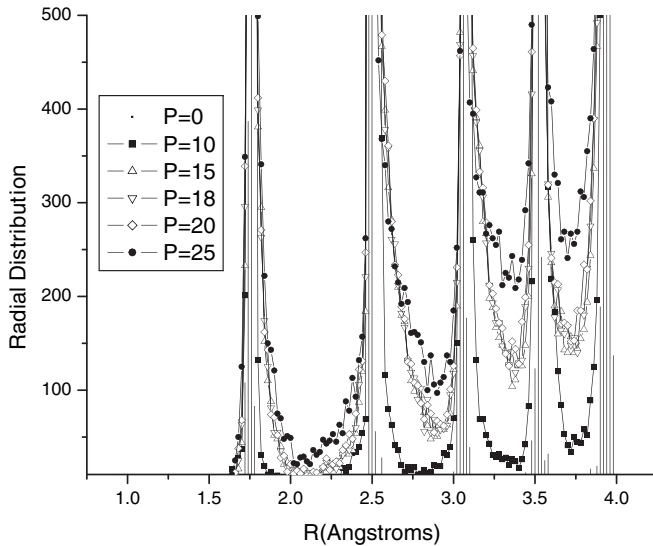


FIG. 3. Calculated radial distribution function of the TiO_2 anatase nanoparticles at various pressures. Vertical bars are for the zero-pressure simulation. Pressure is in units of GPa.

The $P = 0$ GPa result is consistent with what is reported in Ref. [15]. These plots have to be considered as qualitative, recognizing the crude nature of the parameter estimates of the potential used in the MD work. Peak broadening of the RDF is clearly apparent at high pressure indicative of some degree of long-range disorder. In disordered (amorphized) regions of the nanoparticle there can be bond-lengthened configurations as well as the usually expected bond contraction in ordered-crystalline parts at pressure. Within the RDF the one configuration compensates the other and the (weighted) peak positions show a broadening instead of shifting to lower values. The atom distribution within the particle derived from the MD simulations may also be visualized over a sequence of ambient and high pressure conditions; see Fig. 4. At lower pressure there is an onset of a slight lattice distortion mainly about the surface of the nanoparticle. To the highest pressure of 25 GPa, the core of the nanoparticle remains fairly rigid and somewhat crystalline but with some defective structures emerging due to relaxation of the anatase crystal structure. At the highest pressures there appears to be a much higher density of

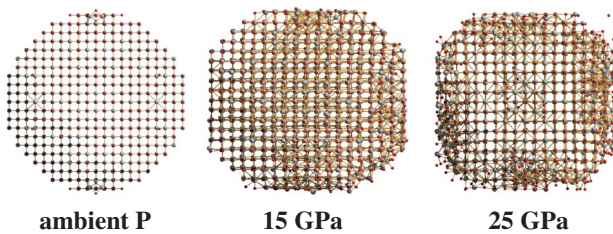


FIG. 4 (color). Atomic geometry within the TiO_2 nanoparticle at various pressures from molecular dynamics simulations. The view is a projection along one of the crystallographic axes of the anatase unit cell.

defect structure in the surface shell than within the core area. Significant disruption of long-range order in this surface shell is signaled by both excessive broadening of the widths of the RDF at the larger radial distances at high pressure (see Fig. 3) and recognizing that a high proportion (30%–40%) of the atoms in the nanosize grain are at the surface. The MD simulations suggest the emergence of disorder in the surface-shell region of the nanograin encapsulating a more crystalline core. This is compatible with persistent signatures of short-range order in the x-ray diffraction (XRD) and Raman data at high pressure; see Figs. 1 and 2. Room-temperature calculations do not influence the overall conclusions of the MD simulations although finite temperature simulations clearly would enhance the RDF peak broadening.

The structures of nanophase materials are dominated by their ultrafine grain sizes and the large number of grain boundaries. Very high stress may occur at the contact points between individual grains at low applied pressures leading to so-called microstrains. It is then difficult to extract absolute values of the unit-cell parameters with any reliability using only powder x-ray diffraction [17,18]. This appears to be the case in our sample up to ~ 6 GPa. We determined the lattice parameter of nanoanatase at each pressure by using the average value calculated from different groups of Bragg reflections in a full-profile fitting of the data [14,17]. Figure 5 shows the measured variation of the relative unit-cell volume of the nanoanatase upon compression. In the pressure range 3–6 GPa the apparent compression of nano- TiO_2 is very low. At pressures higher than 6 GPa the compressibility assumes a different value. This behavior has already been observed for other nanomaterials when the crystallite size is at some critical value below 10 nm [17].

It has also been instructive to monitor the pressure dependence of the FWHM of the most intense (101) peak

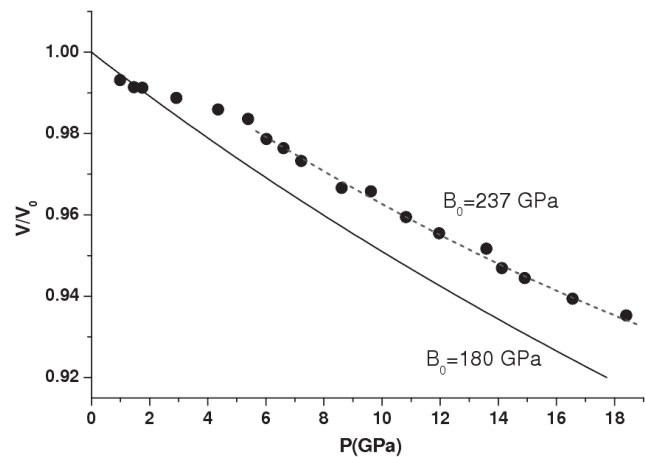


FIG. 5. Relative volume of 6 nm nanoanatase TiO_2 as a function of pressure. The dashed line through the data points is to guide the eye. The lower curve is the extrapolated EOS of bulk anatase with $B_0 = 180$ GPa and $B'_0 = 4$.

(extracted by fitting a Pearson VII function). Upon initial densification, up to 3 GPa, there is a rapid increase in the FWHM perhaps confirming the effect of microstrains. This broadening is also accompanied by a shift of the peak positions, and the average lattice parameter of a nanograin perhaps cannot be obtained reliably. Between 3 and 6 GPa there is almost no variation in the width of the peak. In the range 6–18 GPa there is only a weak monotonic increase of the FWHM, perhaps indicative of less microstrains and consequently more quasihydrostatic conditions [18]. At $P \sim 18$ GPa there is an abrupt increase in FWHM of the (101) Bragg peak accompanied by a drastic loss in intensity, signifying the onset of some degree of disruption of crystallinity in the sample. The pressure evolution of the Raman profiles is similar to the XRD pressure data of Fig. 1. In the pressure range 6–18 GPa, the linewidth of the E_{1g} mode shown in Fig. 2 increases monotonically from 35 to 70 cm^{-1} . This twofold increase in linewidth is consistent with previous Raman pressure studies of nanoanatase [8,9]. At $P \geq 18$ GPa the pressure dependence of the E_{1g} linewidth increases markedly. Beyond 18 up to 23 GPa, which is the highest pressure attained for this Raman study, progressively weaker and broader Raman E_{1g} and ($A_{1g} + B_{1g2}$) anatase modes only (at $\sim 200 \text{ cm}^{-1}$ and $\sim 550 \text{ cm}^{-1}$ in Fig. 2) may still be discerned in the Raman spectra. There is no evidence of a transformation to other (α - PbO_2 or baddeleyite) crystalline phases at pressures beyond 18 GPa. Weak signatures of persistent (anatase) crystallinity at $P > 18$ GPa in both the XRD and Raman data suggest a picture of short-range order in coexistence with appreciable disorder on longer length scales of a few nm.

In the range 6–18 GPa the relative change of the unit-cell volume versus pressure is appreciably lower for the nanophase material compared with the bulk analog; see Fig. 5. A Birch-Murnaghan fit to the nanoanatase data of this pressure range yields a zero-pressure bulk modulus $B_0 = 237 \pm 3$ GPa [third-order equation of state (EOS) with pressure derivative $B'_0 = 4$ fixed, and error representing one standard deviation]. This value is enhanced in comparison with $B_0 = 180$ GPa for the bulk compound at 300 K [19]. The $B_0 = 237$ GPa value is close to that reported for nanoanatase having 30 nm average grain sizes [10]. Therefore as the grain size decreases in anatase the bulk modulus (and therefore likely the hardness and stiffness) increases monotonically to eventually plateau for grain sizes less than $d \sim 30$ nm. The fractional volume reduction at pressure from the MD calculations is 0.956 for $P = 15$ GPa corresponding to a bulk modulus $B_0 = 260$ GPa and 0.945 for $P = 20$ GPa corresponding to $B_0 = 240$ GPa (for fixed $B'_0 = 4$), consistent with experiment.

In conclusion, the ultrastability of the $d \sim 6$ nm version of nanoanatase may be rationalized in terms of nucleation

and growth criteria [9]. The crystalline component has dimensions comparable to or smaller than a critical diameter $d^* \sim 4$ nm, and thus the emergence of the baddeleyite (or any other) crystalline phase at high pressure is not energetically favorable. The compressibility is also deduced to be much ($\sim 30\%$) lower, and the ultrafine nanoanatase is therefore much stiffer, than its macrocrystalline counterpart. Widespread new applications (of what is already a well known wide band-gap semiconductor) that exploit the attributes of ultrafine grain size, ultrastability, and enhanced stiffness may now be envisaged.

This work has been supported by the NRF (South Africa). We are grateful to P. Franklin who provided the samples, to R. Erasmus and Y. Amiel for assistance with Raman and x-ray data collections, respectively, and to F. R. L. Schoning for constructive discussions.

-
- [1] U. Bach *et al.*, Nature (London) **395**, 583 (1998); M. Grätzel, J. Photochem. Photobiol. C **4**, 145 (2003).
 - [2] M. Valden, X. Lai, and D. W. Goodman, Science **281**, 1647 (1998).
 - [3] K. A. Griffin *et al.*, Phys. Rev. Lett. **94**, 157204 (2005).
 - [4] L. S. Dubrovinsky *et al.*, Nature (London) **410**, 653 (2001).
 - [5] *Nanoparticles and the Environment in Reviews in Mineralogy and Geochemistry*, edited by J. F. Banfield and A. Navrotsky (Mineralogical Society of America, New York, 2001), Vol. 44.
 - [6] M. Stir *et al.*, Nucl. Instrum. Methods Phys. Res., Sect. B **199**, 59 (2003).
 - [7] R. Ahuja and L. S. Dubrovinsky, J. Phys. Condens. Matter **14**, 10 995 (2002).
 - [8] Z. Wang and S. K. Saxena, Solid State Commun. **118**, 75 (2001).
 - [9] G. R. Hearne *et al.*, Phys. Rev. B **70**, 134102 (2004).
 - [10] V. Swamy *et al.*, Solid State Commun. **125**, 111 (2003).
 - [11] V. Swamy *et al.*, Phys. Rev. B **71**, 184302 (2005).
 - [12] H. Yin *et al.*, J. Mater. Chem. **12**, 378 (2002).
 - [13] A. Hammersley, Computer Program FIT2D, ESRF, Grenoble, 1998.
 - [14] A. C. Larson and R. B. V. Dreele, Los Alamos National Laboratory, Technical Report No. LAUR 86-748 (unpublished).
 - [15] A. V. Bandura and J. D. Kubicki, J. Phys. Chem. B **107**, 11 072 (2003).
 - [16] V. Swamy and J. D. Gale, Phys. Rev. B **62**, 5406 (2000).
 - [17] B. Palosz *et al.*, J. Phys. Condens. Matter **16**, S353 (2004).
 - [18] At low pressure parts of the nanoparticle surface area are in contact with the pressure-transmitting fluid while other parts contact neighboring nanoparticles. This nonhydrostatic situation impacts on the Bragg reflection profiles. More quasihydrostatic conditions are expected to ensue upon better compaction of the grains at higher pressures.
 - [19] T. Arlt *et al.*, Phys. Rev. B **61**, 14 414 (2000).